Indoor Received Power Prediction Based on Physical Optics (PO): Simulations and Experimental Validation in Industrial Environment

O. A. Iupikov[1], A. Alayón Glazunov[1,2], M. V. Ivashina[1], M. Bärring[3], B. Johansson[3], U. Engström[4], F. Harrysson[4], M. Friis[5] and J. Stahre[3]

[1]Chalmers, Department of Electrical Engineering, Göteborg, Sweden, oleg.iupikov@chalmers.se, marianna.ivashina@chalmers.se
[2]University of Twente, Department of Electrical Engineering, Enschede, the Netherlands, a.alayonglazunov@utwente.nl
[3]Chalmers, Department of Industrial and Materials Science, Göteborg, Sweden, maja.barring@chalmers.se, bjorn.johansson@chalmers.se, johan.stahre@chalmers.se
[4]Ericsson AB, Sweden, ulrika.engstrom@ericsson.com, fredrik.harrysson@ri.se
[5]SKF AB, Sweden, martin.friis@skf.com

Abstract—This study presents an approach based on Physical Optics computations to predict the receive signal power in an indoor environment. The application in focus pertains the development of highly reliable manufacturing industry processes where wireless communications plays a key role. Our proposed numerical method shows a good agreement with measurement data. It is therefore suggested that Electromagnetic modelling based on computationally efficient Physical Optics algorithms can be used as a complement, an alternative or even a replacement for empirical models requiring time consuming measurement campaigns.

Index Terms—PO simulation, radio link

I. Introduction

The manufacturing industry is facing a technical revolution that will modernize their operations enabled by 5G wireless technologies [1]. The paradigm shift in planning the radio coverage in the industrial environments (prior to installation) will benefit from the new features and technologies, such as Massive MIMO and active beamforming array antennas.

A fundamental challenge is assuring the reliability of the wireless network in terms of much shorter delays and higher throughput. This can be achieved through the proper understanding and the accurate prediction of the propagation of ElectroMagnetic (EM) waves in the indoor manufacturing environment, i.e., the response of the radio propagation channel. This requires an accurate modeling of the deployed antenna system, which shall account for the mutual interactions with its surrounding to cope with EM interference effects, multipath fading and mobility allowing a timely adaptation to the changing environment.

A typical EM environment for indoor industrial use can be described by a set of large geometrical structures (e.g. floor, walls and other objects of metal or concrete materials) and may include a variety of stationary or moving metal objects, e.g. electrical machines. Traditionally, antenna system design for these applications has been handled through a

Fig. 1: A photo of Chalmers Smart Industry (CSI) Laboratory at Chalmers University of Technology, Sweden. The Lab contains many metal objects, such as cable ladders, fire extinguisher, pillars, ventilation system, whiteboard, computer numerical control (CNC) machine, etc.

combination of advanced EM simulation tools and powerful computational platforms. On the other hand, due its complexity, the propagation modeling has mainly relied on empirical or simplified analytic approaches. The 5G technological developments have stimulated a growing interest in applying 3-D numerical simulation tools for planning the industrial radio design, which employ either full-wave or high-frequency asymptotic solutions (where ray-tracing techniques are most common choice) [2]. However, due to the diversity of the considered study cases, today there seems to be no common consensus on what constitutes the most suitable 3D modeling technique(s). Most importantly, there is limited understanding on the required or acceptable propagation model accuracy vs. simulation time for the above high-mobility propagation environments.

The present study aims to improve the above knowledge gap by investigating the applicability of a Physical Optics (PO) based 3D-modeling technique, and verifying its performance for a representative industrial environment. The PO-
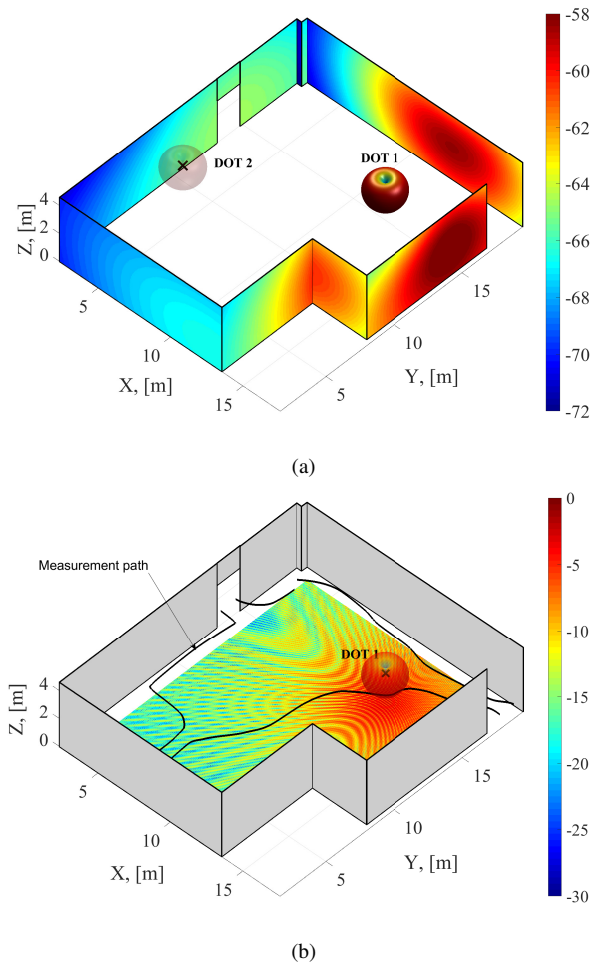
(a)

(b)

Fig. 2: The electromagnetic 3D-model of the CSI lab, overlaid with the simulation results: (a) The PO current distribution (magnitude values) on the PEC walls when the upper transmitting antenna system (DOT 1) is active, in [dBA/m]; while the second antenna (DOT2) is passive; (b) The E-field distribution on the plane elevated 1 m above the floor, in [dB], when both the incident- and scattered field contributions (i.e. the direct contribution of the radio DOT1 and the PO-current produced field, $\boldsymbol{E}_{\text{tot}} = \boldsymbol{E}_{\text{inc}} + \boldsymbol{E}_{\text{scat}}$) are considered; the the black contour denotes the measurement path.

based computations are compared to signal-strength measurements performed in an experimental manufacturing set-up at Chalmers University of Technology by deploying two Radio DOTs and corresponding LTE network infrastructure, all from Ericsson.

II. DESCRIPTION OF THE CSI LABORATORY

Figure 1 shows the Chalmers Smart Industry (CSI) laboratory, which is located at in Gothenburg, Sweden. The material of the walls is a reinforced concrete, therefore we can expect relatively high scattering effects which have been estimated in the order of $-4\ldots-2$ dB in terms of the reflection

coefficient [3]. The dimensions of the lab are $15 \times 18 \times 4$ meters (or $118 \times 142 \times 32\ \lambda$ at the frequency 2.365 GHz).

III. PO-BASED 3-D MODELING APPROACH

Accurate modeling of electrically large and multi-scale electromagnetic problems is a challenging task that is often beyond the capabilities of commercially available simulation tools. To overcome this challenge, we have employed a Physical Optics (PO) based approach to compute the fields scattered from the lab walls and floor, while ignoring the other (smaller) objects in the lab. To enable a time-efficient analysis, we have made the following assumptions:

- Since PO is an asymptotic method, only flat and slowly-curved scatterers are supported (e.g. walls, floor and ceiling of the room). This assumption is not severe for the considered environment, and can be avoided by combining the PO method with other full-wave numerical techniques (e.g. MoM, CBFM, MLFMM, etc.) [4]–[8].
- The materials of the walls, floor and ceiling of the rooms are assumed to be fully metal, and thus can be modeled as perfect electric conductors (PEC). This assumption is generally not valid for any industrial environment and should be analyzed case by case.
- Mutual coupling effects due to the scattering of radio waves in between the walls/floor are negligible. This implies that the E-field value at any point inside the lab (in space or on the walls and the floor) can be computed as the sum of the direct contribution (i.e. incident field from the source such as DOT1 or DOT2) and the field which is scattered from the walls and the floor.
- The radiation pattern of the source (antenna system of DOT1 or DOT2) is assumed to be close to the Gaussian beam pattern (for a linearly-polarized radiator) with the illumination taper of -1 dB at $\theta = 90°$. This taper means that the radiation of the antenna is nearly isotropic in the bottom hemisphere, which illuminates the walls and floor (Fig. 2).

The present PO method has been implemented in MatLab and validated for several bench marking examples in previous projects. For more details on the accuracy and simulation efficiency of this simulation tool, the reader is referred to [4] and [9]. The following simulation settings have been used to analyze the above described lab environment:

- Frequency: 2.365 GHz.
- Size of the EM-problem: ~ 332000 (without the floor) or ~ 640000 (with the floor) mesh cells with the size of $\sim 42 \times 42$ mm ($\sim 0.33 \times 0.33\lambda$).
- The number of radio sources (radio DOTs): two DOTs at different positions on the ceiling, operating either one by one or simultaneously.
- The EM model of the environment consists of 10 walls and the floor
- The E-field power distribution is calculated on the measurement path data to enable comparison.
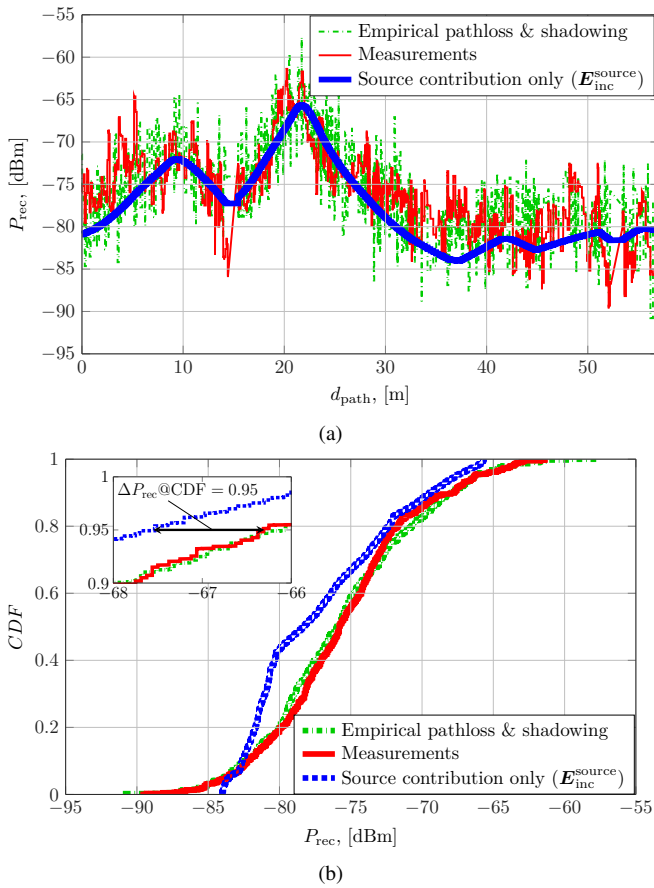
(a)

(b)

Fig. 3: Receive power level (RSRP) along the measurement path. (a) The variations as predicted by the different models are compared with measurements. Results for the direct transmitted field by the antenna (i.e. incident field contribution) are shown for the active Radio DOT 1 active. (b) The corresponding CDFs are plotted.
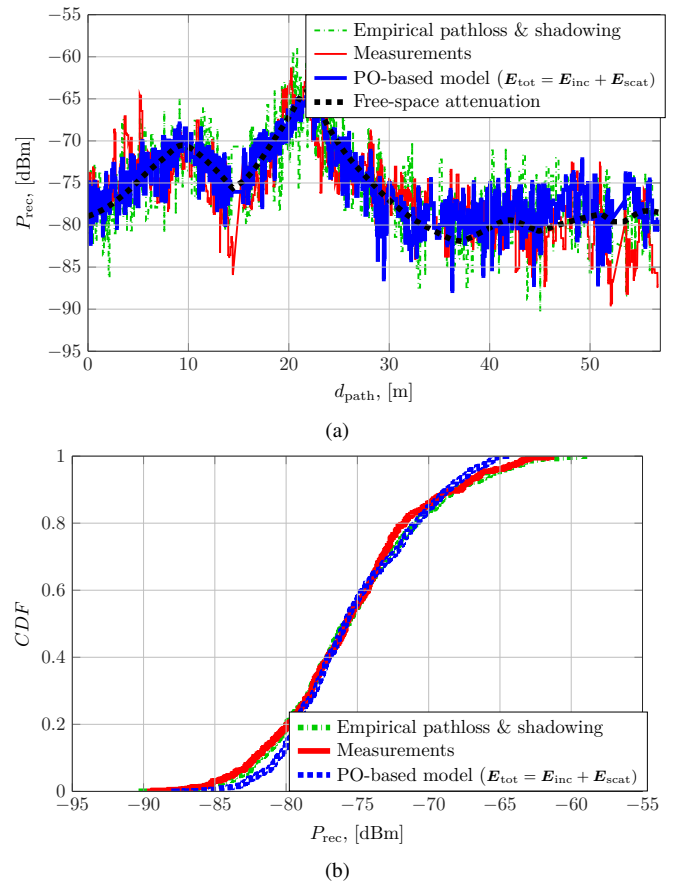

(a)

(b)

Fig. 4: Receive power level (RSRP) along the measurement path. (a) The variations as predicted by the different models are compared with measurements. Results for PO computations are shown for the active upper Radio DOT active. The floor is not included in the model. (b) The corresponding CDFs are plotted.

Fig. 2(a) shows the described geometrical model of the environment, the positions and radiation patterns of the transmitting antennas (DOT 1 and DOT2), and the computed PO current distribution on the walls when the upper radio DOT (DOT 1) is active. Since in this simplified model we have ignored mutual coupling between the walls, the field at any point inside the room can be calculated as the superposition of the field radiated directly by the DOT and the field scattered from the walls (radiated by the PO current): $\boldsymbol{E}_{\text{tot}} = \boldsymbol{E}_{\text{inc}}^{\text{source}} + \boldsymbol{E}_{\text{scat}}^{\text{PO}}$. The magnitude distribution of the resulting E-field on a plane elevated 1 m over the floor is shown on Fig. 2(b) together with the measurement path denoted by the black line.

IV. RESULTS AND DISCUSSION

In the analysis below we compare the models with the measurement data with respect to their means $\mu_{P_{\text{rec}}}$ and standard deviations $\sigma_{P_{\text{rec}}}$. We also evaluate the root mean squared (RMS) error of the simulated data and the measurement data corresponding to the same receive antenna position along the measurement path RMS$_{P_{\text{rec}}}$. The RMS error inferred from

comparing the power corresponding to the same cumulative distribution function (CDF) level RMS$_{P_{\text{rec}}@\text{CDF}}$, [10], is also evaluated as indicated in Fig. 3b. The correlation coefficient ρ between simulated data and the measurement data has also been computed.

To add to the analysis and since empirical pathloss models have been actively used in radio propagation modeling we also compute the above-mentioned figures-of-merit for an empirical channel model [11]. A well-known empirical propagation model is the pathloss plus shadowing computed as

$$L = \alpha + 10\gamma \log_{10}(d_{\text{Tx-Rx}}) + S(0, \sigma_s), \tag{1}$$

where the constant α models the average path loss at a unit distance and depends on the environment, the antennas used and the carrier frequency; γ is the path loss exponent modelling the rate of decay of the average receive power with the separation distance between the receiver and the transmitter $d_{\text{Tx-Rx}}$; $S(0, \sigma_s)$ is a Gaussian random variable with zero mean and standard deviation σ_s, modeling the fluctuations of the receive power at a fixed distance $d_{\text{Tx-Rx}}$ (i.e., fluctuations

TABLE I: Mean and standard deviation of the empirical model, the PO computations and measurement data.

Performance metric of the model	Active radio DOT	Measured data	Empirical model	Source contribution only, $E_{\text{inc}}^{\text{source}}$	$E_{\text{tot}} = E_{\text{inc}}^{\text{source}} + E_{\text{scat}}^{\text{PO}}$	
					w/o floor	with floor
Mean received power, $\mu_{P_{\text{rec}}}$, [dBm]	Lower	-75.1	-75.1	-77.7	-75.7	-74.2
	Upper	-75.5	-75.7	-77.2	-75.2	-73.7
	Both	-70.7	-71.1	-73.0	-70.9	-70.1
Received power standard deviation, $\sigma_{P_{\text{rec}}}$, [dBm]	Lower	5.4	5.4	4.7	4.4	4.1
	Upper	5.2	5.2	5.0	4.5	4.2
	Both	3.5	3.4	3.3	3.1	3.1

TABLE II: Comparison of PO computations and empirical model simulations with measurement data.

Performance metric of the model	Active radio DOT	Empirical model	Source contribution only, $E_{\text{inc}}^{\text{source}}$	$E_{\text{tot}} = E_{\text{inc}}^{\text{source}} + E_{\text{scat}}^{\text{PO}}$	
				w/o floor	with floor
Correlation coefficient, ρ, [-]	Lower	0.7	0.8	0.7	0.7
	Upper	0.6	0.8	0.7	0.6
	Both	0.5	0.7	0.5	0.4
Root mean squared error, $\text{RMS}_{P_{\text{rec}}}$, [dB]	Lower	4.3	4.3	4.3	4.2
	Upper	4.6	3.8	3.8	4.5
	Both	3.3	3.6	3.2	3.6
RMS error inferred from comparing the power corresponding to the same CDF level, $\text{RMS}_{P_{\text{rec}}@\text{CDF}}$, [dB]	Lower	0.8	3.1	1.5	1.7
	Upper	0.5	2.1	1.0	2.2
	Both	0.4	2.3	0.6	0.8

around the mean). The values of α, γ and σ_s are obtained by fitting (1) to the measurement data. Knowing the path loss with shadowing (1) the receive power P_{Rx} is determined using the well-known relationship

$$P_{\text{Rx}} = EIRP_{\text{Tx}} + G_{\text{Rx}} - L, \qquad (2)$$

where $EIRP_{\text{Tx}} = 20$ dBm is the equivalent isotropic radiated power over the channel bandwidth of 20 MHz; G_{Rx} is the gain of the receive antenna which in our case is the antenna of the TEMS pocket LTE mobile phone used with $G_{\text{Rx}} \approx 0$ dBi.

As can be seen from Table I, the empirical model provides results that emulate the measurements very well. Both the mean and the standard deviation obtained with the empirical model are almost identical to corresponding values of measurements, up two a few tenths of dBs. It is worthwhile to mention that these results illustrate a single realization of the empirical model. However, the determination of the confidence for the empirical model is outside the current study. The expected good agreement is further corroborated by Table II, where the RMS error between the empirical model and measurement is shown to be within $3.3 - 4.6$ dB, which is excellent. Also a rather high correlation between simulations and measurement data can be observed, i.e., $0.5 - 0.7$. The probability distributions derived from the measurements and the empirical model are also in rather good agreement with RMS errors of the powers corresponding to the same CDF-level within $0.4 - 0.8$ dB.

As the focus of the paper is the analysis of the performance of PO computations we provide similar parameters in Tables I and II as for the empirical simulations. In our model we model the walls of the production workshop as a PEC material. We also investigate the impact of the floor (also PEC).

From Table I we can see that PO computations with no floor model (i.e., walls only) provide almost the same average

receive power as in measurements (see Fig.4). Furthermore, on one hand, when no scattered field ($E_{\text{scat}}^{\text{PO}}$) is included, the receive power is lower and behaves similarly to the free-space channel since the radiation pattern of the DOT antenna is nearly uniform over a hemisphere (see Fig. 3). This is expected since only the direct transmit power of the active Radio DOT ($E_{\text{inc}}^{\text{source}}$) contributes to the total received power. The discrepancy can be attributed to both modelling and measurement uncertainties. On the other hand, when the PO contribution is added, the power level increases due to field reverberation effects (see Fig. 4). Now, by introducing the PEC floor, the average power increases for the case with PO contribution since more power (reflected from the PEC floor) is contributed into the simulation volume. In all cases the correlation remains high due to the ability to emulate the average distance dependence trend of the receive power.

It is worth mentioning that the simulation time in the current code implementation in Matlab is about 3 sec to compute the PO currents and about 10 ms per point where the field should be calculated, which is much faster than performing measurements for the empirical model, using ray-tracing or any full-wave solvers. The time-efficient computations can facilitate fast re-estimation of the channel when the indoor environment changes.

V. CONCLUSION

We have shown that in a line-of-sight (LoS) indoor environment it's sufficient to consider perfect electric conductive (PEC) walls and no floors in the considered indoor environment in both absolute terms as well as in statistical terms, i.e., its cumulative distribution function. The main advantage of this simple model compared to the empirical model is that it doesn't require measurements, significantly reducing

the analysis time, and allowing for prediction of the received power when the indoor environment changes.

REFERENCES

[1] S. Wang, J. Wan, D. Li, and C. Zhang, "Implementing smart factory of industrie 4.0: An outlook," *International Journal of Distributed Sensor Networks*, vol. 12, no. 1, pp. 1–10, 2016.

[2] J. Pascual, J.-M. Molina, M.-T. Martinez-Ingles, J.-V. Rodríguez, and L. Juan-Llácer, "Wireless channel simulations using geometrical models extracted from point clouds," Eurpean Cooperation in Science and Technology, Euro-COST, Centro Universitario de la Defensa, Universidad Politécnica de Cartagena (Spain), Technical Report, Jan. 2018.

[3] R. A. Dalke, C. L. Holloway, P. McKenna, M. Johansson, and A. S. Ali, "Effects of reinforced concrete structures on rf communications," *IEEE Transactions on Electromagnetic Compatibility*, vol. 42, no. 4, pp. 486–496, Nov. 2000.

[4] O. A. Iupikov, R. Maaskant, M. Ivashina, A. Young, and P. Kildal, "Fast and accurate analysis of reflector antennas with phased array feeds including multiple reflections between feed and reflector," *IEEE Trans. Antennas Propag.*, vol. 62, no. 7, Jul. 2014.

[5] C. D. Giovampaola, E. Martini, A. Toccafondi, and S. Maci, "A hybrid PO/generalized-scattering-matrix approach for estimating the reflector induced mismatch," *IEEE Trans. Antennas Propag.*, vol. 60, no. 9, pp. 4316–4325, Sep. 2012.

[6] J. M. Taboada and F. Obelleiro, "Including multibounce effects in the moment-method physical-optics (MMPO) method," *Micr. Opt. Technol.*, vol. 32, no. 6, pp. 435–439, 2002.

[7] U. Jakobus and F. M. Landstorfer, "Improved PO-MM hybrid formulation for scattering from three-dimensional perfectly conducting bodies of arbitrary shape," *IEEE Trans. Antennas Propag.*, vol. 43, no. 2, pp. 162–169, Feb. 1995.

[8] R. Maaskant, M. V. Ivashina, O. Iupikov, E. A. Redkina, S. Kasturi, and D. H. Schaubert, "Analysis of large microstrip-fed tapered slot antenna arrays by combining electrodynamic and quasi-static field models," *IEEE Trans. Antennas Propag.*, vol. 56, no. 6, pp. 1798–1807, Jun. 2011.

[9] O. Iupikov, "Digital beamforming focal plane arrays for radio astronomy and space-borne passive remote sensing," PhD Thesis, Institutionen för signaler och system, Antenner, Chalmers tekniska högskola, Göteborg, Jun. 2017. [Online]. Available: http://publications.lib.chalmers.se/records/fulltext/249055/249055.pdf

[10] P.-S. Kildal, *Foundations of Antenna Engineering – A Unified Approach for Line-Of-Sight and Multipath*. Kildal Antenn AB, 2015.

[11] G. de la Roche, A. A. Glazunov, and B. Allen, *LTE-Advanced and Next Generation Wireless Networks – Channel Modelling and Propagation*. Chichester, U.K.: Wiley, 2012.